OPEN ACCESS Freely available online

PLoS one

Aβ Peptide Fibrillar Architectures Controlled by Conformational Constraints of the Monomer

Kristoffer Brännström[1], Anders Öhman[2]*, Anders Olofsson[1]*

1 Department of Medical Biochemistry and Biophysics, Umeå University, Umeå, Sweden, **2** Department of Chemistry, Umeå University, Umeå, Sweden

Abstract

Anomalous self-assembly of the Aβ peptide into fibrillar amyloid deposits is strongly correlated with the development of Alzheimer's disease. Aβ fibril extension follows a template guided "dock and lock" mechanism where polymerisation is catalysed by the fibrillar ends. Using surface plasmon resonance (SPR) and quenched hydrogen-deuterium exchange NMR (H/D-exchange NMR), we have analysed the fibrillar structure and polymerisation properties of both the highly aggregation prone Aβ1–40 Glu22Gly ($Aβ^{40Arc}$) and wild type Aβ1–40 ($Aβ^{40WT}$). The solvent protection patterns from H/D exchange experiments suggest very similar structures of the fibrillar forms. However, through cross-seeding experiments monitored by SPR, we found that the monomeric form of $Aβ^{40WT}$ is significantly impaired to acquire the fibrillar architecture of $Aβ^{40Arc}$. A detailed characterisation demonstrated that $Aβ^{40WT}$ has a restricted ability to dock and isomerise with high binding affinity onto $Aβ^{40Arc}$ fibrils. These results have general implications for the process of fibril assembly, where the rate of polymerisation, and consequently the architecture of the formed fibrils, is restricted by conformational constraints of the monomers. Interestingly, we also found that the kinetic rate of fibril formation rather than the thermodynamically lowest energy state determines the overall fibrillar structure.

Citation: Brännström K, Öhman A, Olofsson A (2011) Aβ Peptide Fibrillar Architectures Controlled by Conformational Constraints of the Monomer. PLoS ONE 6(9): e25157. doi:10.1371/journal.pone.0025157

Editor: Edathara Abraham, University of Arkansas for Medical Sciences, United States of America

Received June 9, 2011; **Accepted** August 26, 2011; **Published** September 29, 2011

Funding: This work was supported by J.C. Kempe Foundation, the Swedish Research Council, O.E. och Edla Johanssons vetenskapliga stiftelse, FAMY and the Medical Faculty of Umeå University. The funders had no role in study design, data collection and analysis, decision to publish, or preparation of the manuscript.

Competing Interests: A.O. is a shareholder of AlexoTech AB. AlexoTech AB had no role in study design, data collection and analysis, decision to publish, or preparation of the manuscript and does not in any other way interfere with the study. This does not alter the authors' adherence to all the PLoS ONE policies on sharing data and materials.

* E-mail: anders.ohman@chem.umu.se (AÖ); anders.olofsson@medchem.umu.se (AO)

Introduction

Alzheimer's disease (AD) is the most common form of dementia today and results in both individual suffering and major economical costs for society [1]. Development of AD is strongly correlated to aggregation and amyloid formation of the 38–43 residue long amyloid-β peptide (Aβ). Aβ peptide is derived via sequential cleavages of the amyloid precursor protein (APP) by β- and γ-secretases and is a natively unfolded peptide having a high propensity to aggregate into cross-β amyloid fibrils through a nucleation-dependent mechanism. The reason why Aβ peptides detrimentally self-assemble into fibrils in certain individuals is currently not well understood. In most AD cases, no underlying factor for the development of the disease can be pinpointed. However, within a small group of individuals with early onset Alzheimer's disease (EOAD), a Mendelian inheritance has been observed [2]. For most of these cases, a genetic anomaly results in an enhanced processing of APP followed by increased Aβ levels, ultimately resulting in an increased rate of aggregation and fibril formation [3]. In a few cases of EOAD, the phenotype has been linked to a mutation within the Aβ sequence of the APP gene resulting in a gain of function where increased aggregation is observed. The Aβ Glu22Gly mutation was identified in northern Sweden and is frequently denoted as the Arctic Aβ variant, $Aβ^{40Arc}$. This mutation is associated with an aggressive form of AD [4,5,6]. Aβ Glu22Gly has a very high propensity for aggregation and an enhanced ability to form protofibrils that have been shown to be cytotoxic in both cell culture and transgenic animals [5,7,8,9,10,11,12,13].

Amyloid polymerisation is a complicated process where monomers are incorporated into the amyloid fibril form in several steps. The polymerisation process has been studied in detail and it is widely accepted that the process involves a dock and lock mechanism [14]. The accepted model involves an initial docking step that is followed by an affinity maturation reaction through an isomerisation phase resulting in adjustment into a conformation with higher binding strength. The model has been further developed into 3 steps based on a dock, lock and block mechanism where an initial weak association is followed by a time dependent maturation phase with a concomitant increase in binding affinity [15]. As each subunit is incorporated, a novel recognition site is created and subsequent binding of additional peptides blocks dissociation. This polymerisation phenomenon can be conveniently monitored using surface plasmon resonance (SPR) where pre-formed fibrils are immobilised and polymerisation is monitored through the addition of monomeric Aβ peptides [15,16,17,18].

Within this work we can show that the architecture of Aβ fibrils is determined by constraints imposed by the monomer conformation during docking and isomerisation. This finding has general implications and suggests that although Aβ is considered to be unstructured it is restrained to adopt certain conformations which impair its ability to acquire certain fibrillar structures. Interestingly, our results moreover show that the kinetic rate of fibril

formation determines the fibrillar architecture rather than the thermodynamically lowest energy state.

Materials and Methods

Preparation of monomeric peptide and fibrillar samples

All peptides were obtained from Alexotech AB, Umeå, Sweden (www.alexotech.com). Due to the aggregation properties of Aβ-peptides, an appropriate solubilisation scheme was essential. Prior to use, lyophilised peptides were solubilised in 10 mM NaOH at pH 12, followed by 30 s sonication in a water bath and 5 min centrifugation at 20 000 g to remove residual oligomeric species. This treatment efficiently monomerised the peptides and facilitated dilution in phosphate buffered saline (PBS, 15 mM phosphate buffer, pH 7.4, 150 mM NaCl) to the selected concentrations. All samples were verified to have pH 7.4 or a pD corresponding to 7.0 by direct pH meter reading. Fibrillar forms were acquired by incubating 100 μM Aβ at 37°C under agitation for 48 hours. μ.

H/D exchange and NMR analysis of $A\beta^{40WT}$ and $A\beta^{40Arc}$ fibrils

The fibrillar forms of ^{15}N-$A\beta^{40WT}$ and ^{15}N-$A\beta^{40Arc}$ were prepared as described above. Fibrils composed of ^{15}N-$A\beta^{40Arc}$ were also prepared by cross-seeding using 15% (w/w) ^{14}N-$A\beta^{WT40}$ fibrils as seeds. Agitation was omitted during cross-seeding experiments.

To probe solvent accessibility, aggregate/fibrillar solutions of each peptide type were split into two fractions and recovered by short centrifugation at 20 000 g. Hydrogen-deuterium (H/D) exchange was carried out on one of the fractions by diluting the pellets 30 times using a D_2O solution (20 mM Tris, 150 mM NaCl, pD 7.0) followed by 24 h incubation at 37°C. The second fraction was used without further treatment as a fully protonated reference sample to identify and exclude amide exchange resulting from the experimental procedure (i.e. highly exposed amides within the monomeric state). At the end of the incubation period and immediately prior to NMR analysis, Aβ assemblies were recovered by short centrifugations (20 000 g) and rapidly converted into NMR-detectable monomers using an optimised solution of hexafluoroisopropanol as described previously [19].

Hydrogen exchange was subsequently monitored by recording a series of heteronuclear 2D ^{15}N-HSQC experiments, typically starting 6–8 minutes after fibril dissolution. All experiments were performed at 15°C on a 600 MHz Bruker AVANCE spectrometer, equipped with a 5 mm triple-resonance, pulsed-field z-gradient cryoprobe. The acquisition time for each ^{15}N-HSQC experiment was 10 min using four transients per increment and 128 (t_1)×1024 (t_2) complex data points. Prior to each ^{15}N-HSQC experiment, a 1D proton NMR spectrum was acquired to quantitatively monitor the dissolution of fibrils into monomers. Protection ratios and experimental errors were determined as described previously [19,20,21,22,23,24,25].

Surface plasmon resonance (SPR)

The different Aβ variants, including both monomeric and fibrillar, forms were immobilized at 10 μM peptide concentration to a final density corresponding to 2000–5 000 RU to a CM5 chip or to the dextran free chip C1 (GE Healthcare) using standard amine-coupling chemistry at pH 5. Briefly, to activate the chip a 50/50 mixture of EDC (*N*-(3-dimethylaminopropyl)-*N*′-ethylcarbodimidehydrochloride) 0.4 M and NHS (*N*-hydroxysuccinimide) 0,1 M for 7 min.

After immobilization the chip was inactivated with a 7 min injection of etanolamine 1 M.

Analysis of monomeric Aβ binding to fibrils was performed at a flow rate of 20 μl/min in PBS at 25°C. Important to note is that the SPR signal is affected by the physical distance of the analyzed interaction and the chip-surface. Due to the intrinsic nature of a polymerising reaction the distance between the fibrillar ends and the surface will increase during the reaction. Upon extended polymerisation this results in a decreasing SPR signal and a non-linear response. This effect was in detail monitored and to avoid the problem of a non-linear dependency, fibrillar extension was kept at a minimum, using short injection times in combination with low peptide concentration, well within the range where a non-linear curvature becomes pronounced.

According to standard procedures all sensograms were corrected for non-specific interactions to a reference surface, and by double referencing [26]. Regarding a subsequent analysis of the fibril morphology Aβ fibrils were immobilized to 1000RU on a C1 chip followed by injection of monomeric Aβ allowing the fibrils to grow to at least 3000RU. The SPR chip was then dissembled and directly analyzed using AFM as described below.

Affinity determination between free peptide and the amyloid fiber using SPR

Measurements of binding affinities between free monomers and an amyloid fibril is not straight forwards since saturation of monomer binding cannot be reached. However, since the concentration of fibrils is constant during polymerisation, the monomer dissociation constant will be equal to the free concentration (critical concentration) of monomers at equilibrium. Therefore, the dissociation constant can be used in combination with SPR data obtained with known concentrations of peptides in the running buffer to determine the affinity between the monomers and fibrillar ends [27,28]. Fibril extension of Aβ was initiated through injection of 2 μM onto preformed immobilized fibrils at a flow rate of 20 μl/min in PBS at 25°C for in total 30 s followed immediately by various injection of 0–400 nM Aβ solution using the feature COINJECTION. The specific concentration of Aβ in the second injection that produced a linear plateau response (no dissociation observed) represent the critical concentration for polymerisation and consequently also the binding constant.

Atomic force microscopy (AFM) analysis

Fibrillar samples were analysed directly on the surface of C1 chips (GE Healthcare, Uppsala, Sweden) that do not have a dextran surface. Analysis was performed using a Nanoscope IIIa multimode AFM (Digital Instruments Santa Barbara, USA) in tapping mode™ in air. A silicon probe was oscillated at around 280 kHz and images were collected at an optimised scan rate corresponding to 1–2 Hz.

Results

Fibrillar core analysis using quenched H/D exchange NMR

To evaluate whether there are any structural differences between the fibrillar cores of $A\beta^{40Arc}$ and $A\beta^{40WT}$, their corresponding fibrillar form were analysed through quenched H/D exchange NMR experiments. Figure 1a and 1b illustrates the solvent protection of the core structure of $A\beta^{40Arc}$ and $A\beta^{40WT}$, respectively. The result clearly shows that no significant difference can be identified between the two forms, only a slightly lower protection is observed for the four C-terminal residues of $A\beta^{40WT}$. Figure 1c illustrates the H/D exchange pattern acquired from $A\beta^{40Arc}$ when seeded with $A\beta^{40WT}$ fibrils and further strengthen

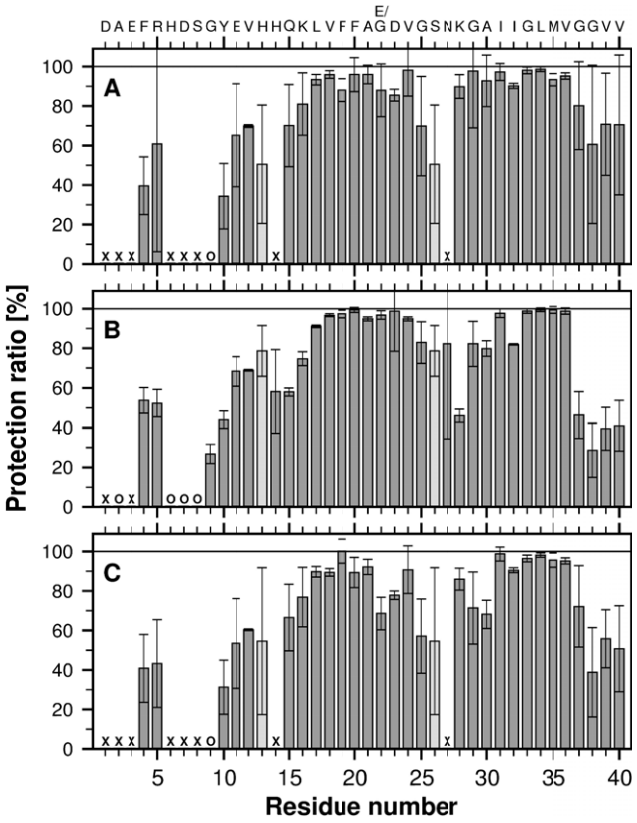

Figure 1. Solvent protection ratios for backbone amide protons as determined by quenched H/D exchange monitored by NMR spectroscopy. Protection is defined as the ratio of the observed signal intensity after a 24 h pre-incubation period in D_2O to the signal intensity in a completely protonated reference sample. Protection in the reference sample is defined as 100%. Circles correspond to residues with 0% protection and crosses to residues where exchange was too fast for detection. Pale grey bars indicate overlapping residues with ambiguously assigned protection ratios. Error bars indicate the experimental uncertainty given by the measurements. (A) $A\beta^{40Arc}$ fibrils, (B) $A\beta^{40WT}$ fibrils, and (C) $A\beta^{40Arc}$ seeded with $A\beta^{40WT}$ fibrils.
doi:10.1371/journal.pone.0025157.g001

the notion that no obvious difference can be detected on the backbone structure, apart from a moderate reduction of the solvent protection at the mutation site of $A\beta^{40Arc}$.

Fibril polymerisation of $A\beta^{40WT}$ and $A\beta^{40Arc}$ monitored by SPR

Surface plasmon resonance (SPR) enables the changes in bound mass to a surface to be monitored and therefore provides a convenient tool to follow fibril formation. Immobilised $A\beta^{40WT}$ fibrils recruited free $A\beta^{40WT}$ monomers by a fibrillar polymerisation process (Fig. 2a). Binding sensograms hence displayed an association phase immediately upon injection of monomeric Aβ peptides as a result of a continuous polymerisation, followed by a dissociation phase at the end of each injection. The same result was observed for immobilised fibrils of $A\beta^{40Arc}$ and free $A\beta^{40Arc}$ monomers (Fig. 2b). To further examine the intermolecular interactions between $A\beta^{40WT}$ and $A\beta^{40Arc}$, cross-seeding experiments were also performed. Interestingly, only a very slow polymerisation was observed upon exposing monomeric $A\beta^{40WT}$ to $A\beta^{40Arc}$ fibrils accompanied by a more rapid dissociation phase (Fig. 2c). In contrast, $A\beta^{40Arc}$ monomers were easily recruited by $A\beta^{40WT}$ fibrils and not accompanied with an increase in dissociation rates (Fig. 2d). The effects on polymerisation and dissociation rates for $A\beta^{40WT}$ monomers persisted even after cross-seeding with $A\beta^{40Arc}$/$A\beta^{WT40}$ fibrils suggesting that it is the fibrillar architecture rather than a sequence specific effect that is causing this effect (data not shown). As a consequence, two different fibrillar architectures can be anticipated where $A\beta^{40Arc}$ monomers can more easily polymerise onto either fibrillar form than $A\beta^{40WT}$ monomers.

Immobilised monomeric Aβ on the chip surface could not recruit monomeric variants from the solution, probed in an identical manner as described above. This important control verified the specificity of the system and also highlights the dependency of a specific structure for an efficient peptide assembly (data not shown).

Ultra-structure of $A\beta^{40WT}$ and $A\beta^{40Arc}$ fibrils

An SPR chip without dextran (C1, GE Healthcare, Uppsala Sweden) was employed to compare $A\beta^{40WT}$ and $A\beta^{40Arc}$ fibril morphologies and verify preservation of fibril integrity during immobilisation on the SPR chip. Sonicated fibrils of $A\beta^{40WT}$ or $A\beta^{40Arc}$ were immobilised followed by a continuous polymerisation. The surface of the C1 chips were directly analysed using AFM (Fig. 3). The predominant fibrillar morphology had a diameter of 5 nm but all samples also contained thinner filaments of 3 nm diameter. No significant differences in morphology between the different samples were observed.

$A\beta^{40Arc}$ displays stronger binding to fibrils than $A\beta^{40WT}$

The critical concentration of free monomers at equilibrium was determined by SPR using a co-injection technique where the dissociation phase is monitored and modulated after monomer injection by varying the concentrations of monomer in the running buffer during the decay phase [29]. The KD50 for monomeric $A\beta^{40WT}$ and $A\beta^{40WT}$ fibrils was determined to be 200 nM (Fig. 4a). This result is consistent with a previous report [29]. The KD50 for monomeric $A\beta^{40Arc}$ and $A\beta^{40Arc}$ fibrils was slightly higher (100 nM, Fig. 4b). Surprisingly, binding of monomeric $A\beta^{40Arc}$ to $A\beta^{40WT}$ fibrils had the strongest interaction with a KD50 value of 50 nM (Fig. 4c).

Docking and isomerisation of $A\beta^{40Arc}$ is enhanced

The finding of an impaired ability for of $A\beta^{40WT}$ to adopt the fibrillar architecture of $A\beta^{40Arc}$ fibrils implies an energetic barrier. According to the principle of a template- dependent dock and lock mechanisms, the locking of a peptide cannot efficiently occur unless the previously loaded peptide has assembled into the correct position [14,15]. A scenario where locking of the peptide (i.e. affinity maturation), is the rate limiting step would be pronounced at higher peptide concentrations and decrease at lower concentrations peptide concentrations. The concentration dependence of fibril polymerisation was hence investigated to determine if peptide locking is a rate limiting step. A clear difference in association rates was observed when different concentrations of monomeric $A\beta^{40WT}$ were polymerised with $A\beta^{40Arc}$ or $A\beta^{40WT}$ fibrils (Fig. 5a). However, the relative difference in association rate was not reduced at lower concentrations upon comparing the two different systems. This can be seen as a linear dependence of the association rate versus different concentrations. A system where the isomerisation rate is rate limiting would result in a non-linear curve. This indicates that a prolonged isomerisation phase, as a result of lower monomeric concentrations, did not diminish the effect on association rates. Regarding the interaction between $A\beta^{40WT}$ monomers and $A\beta^{40Arc}$ fibrils the rate of assembly could

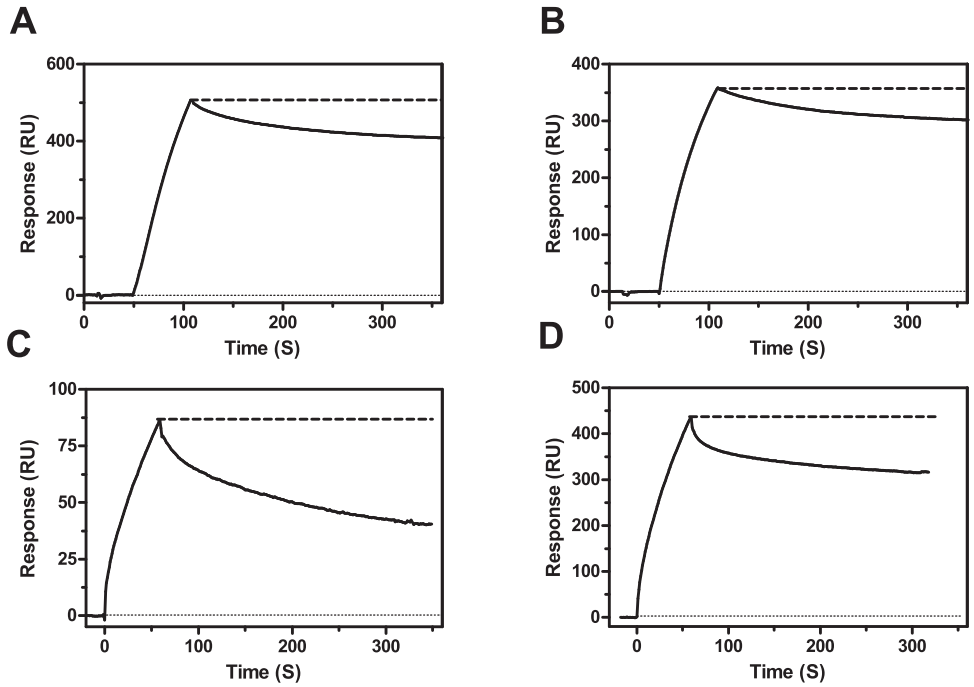

Figure 2. SPR study of fibril elongation. Pre-formed Aβ fibrils were immobilised on a CM5 chip and probed with 2 μM monomeric Aβ for 1 min at a flow rate of 20 μl/min in PBS at 25°C. (A) Monomeric $A\beta^{40WT}$ seeded with $A\beta^{40WT}$ fibrils, (B) monomeric $A\beta^{40Arc}$ seeded with $A\beta^{40Arc}$ fibrils, (C) monomeric $A\beta^{40WT}$ seeded with $A\beta^{40Arc}$ fibrils, and (D) monomeric $A\beta^{40Arc}$ seeded with $A\beta^{40WT}$ fibrils.
doi:10.1371/journal.pone.0025157.g002

not be monitored below 500 nM and a likely explanation is that the concentration corresponding to the KD of the interaction is reached. Although the KD value for the interaction between free $A\beta^{40WT}$ monomer and $A\beta^{40Arc}$ fibrils could not be determined as the signal to noise ratio was too low this a higher KD value is supported by an increased level of dissociation (Fig. 2c) suggesting looser interactions and a competing back-reaction during the isomerisation step.

A competition study was moreover carried out to investigate the different docking abilities of $A\beta^{40WT}$ and $A\beta^{40Arc}$ monomers on $A\beta^{40Arc}$ fibrils (Fig. 5b). The results indicate that $A\beta^{40WT}$ monomer docking cannot compete with $A\beta^{40Arc}$ monomer docking onto $A\beta^{40Arc}$ fibrils, indicating an impaired ability of $A\beta^{40WT}$ to dock with $A\beta^{40Arc}$ fibrils. The decay rate is however, affected suggesting that a fraction of incorporated $A\beta40^{WT}$ significantly interferes with the overall stability of the fibril.

Discussion

To fully understand the self-assembly of Aβ fibrils with the ultimate goal of inhibiting Aβ formation as a treatment for AD, it is important to characterise both the fibril structural architecture and the mechanisms of fibril formation. The intrinsic properties of amyloid fibrils make a detailed molecular characterisation technically challenging and the classical methods for structural elucidation, such as X-ray crystallography and solution NMR, cannot be directly applied. We have therefore developed a methodology based on quenched H/D exchange combined with

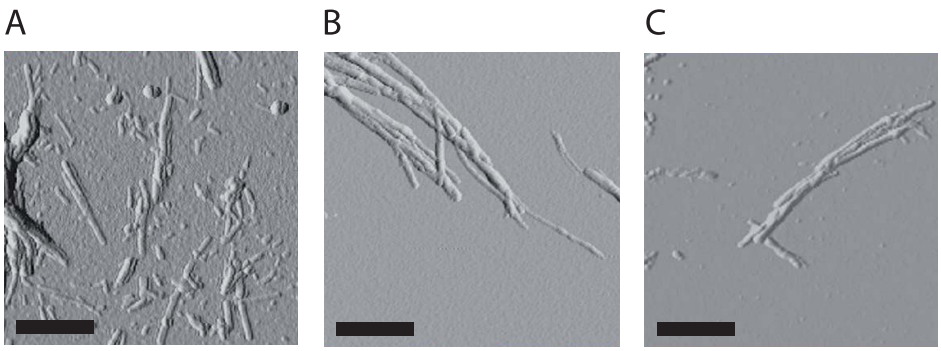

Figure 3. AFM analysis of fibrils immobilised on a C1 chip. Mature fibrils were briefly sonicated prior to immobilisation on C1 chip followed by continuous polymerisation with free monomers until the total mass doubled. (A) Monomeric $A\beta^{40WT}$ seeded with $A\beta^{40WT}$ fibrils, (B) monomeric $A\beta^{40Arc}$ seeded with $A\beta^{40Arc}$ fibrils, and (C) monomeric $A\beta^{40Arc}$ seeded with $A\beta^{40WT}$ fibrils. Scale bar is 0.5 μm.
doi:10.1371/journal.pone.0025157.g003

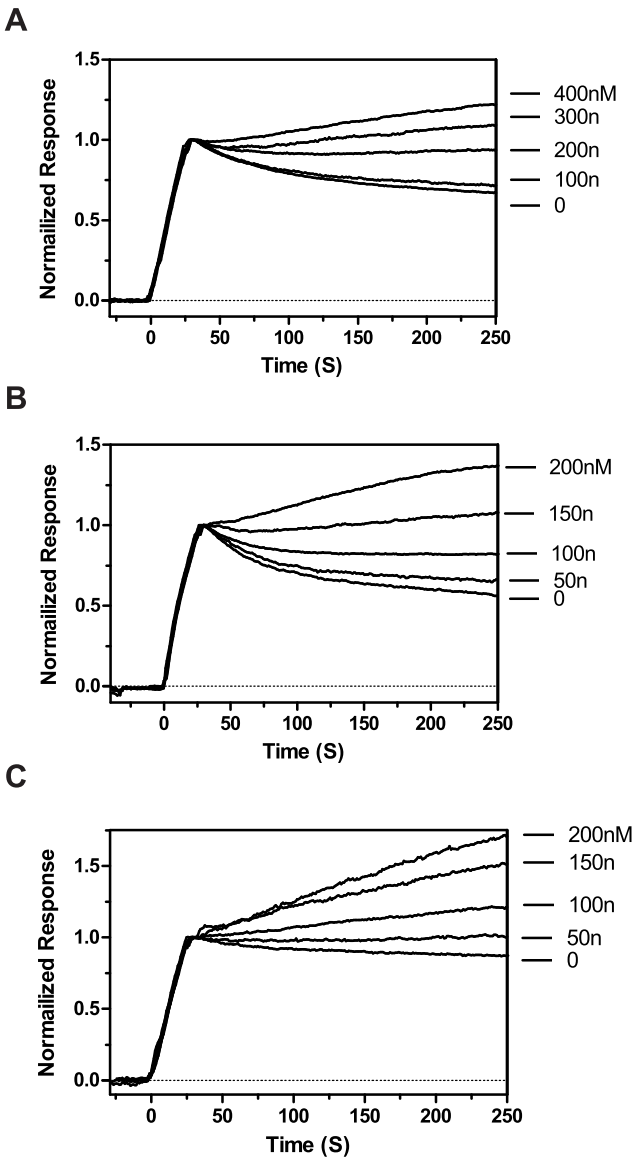

Figure 4. Determination of the critical free concentration of Aβ required for fibril polymerisation. 2 μM Aβ solution was injected for 30 s at a flow rate of 20 μl/min in PBS at 25°C. 100 μl of Aβ (0–400 nM) was then immediately injected. Measurements were carried out to determine the critical free concentrations for (A) $A\beta^{40WT}$ monomers with $A\beta^{40WT}$ fibrils, (B) $A\beta^{40Arc}$ monomers with $A\beta^{40Arc}$ fibrils, and (C) $A\beta^{40Arc}$ monomers with $A\beta^{40WT}$ fibrils.
doi:10.1371/journal.pone.0025157.g004

NMR spectroscopy to monitor the architecture and dynamics of Aβ fibril assemblies. The method quantitatively identifies the residues involved in the fibrillar core [19,20,21,22,23]. Using solvent protection analysis, we can conclude that the fibrillar architectures of $A\beta^{40WT}$ and $A\beta^{40Arc}$ are strikingly similar, with only minor differences for residues at the mutation site and the C-terminal end. However, detailed analysis of the fibril formation kinetics showed that $A\beta^{40WT}$ and $A\beta^{40Arc}$ fibril types differ in their ability to template a polymerisation reaction.

The results presented here from cross-seeding experiments show that monomeric $A\beta^{40Arc}$ cross-reacted easily with fibrils formed by $A\beta^{40WT}$. This is likely a result of the higher freedom of motion due to the introduction of glycine at position 22. $A\beta^{40WT}$ was easily incorporated within the fibrillar form of $A\beta^{40WT}$ but not $A\beta^{40Arc}$. Through kinetic analysis, we showed that $A\beta^{40WT}$ seeded on $A\beta^{40Arc}$ exhibited a higher dissociation rate, indicating a competing back-reaction where alternative conformations results in increased dissociation of the monomer from the fibril. A preceding cross-seeding event did not change the behaviour, suggesting that the effect is a consequence of the fibrillar architecture rather than the specific monomer sequence.

In the dock and lock model, the addition of a peptide onto the fibrillar end is energetically unfavourable unless the previous peptide has adopted the fibrillar conformation. This means that prolongation of the maturation step (i.e. the time between incorporation of two subsequent peptides onto the fibril) would favour an increase in the fraction of high affinity bound peptides. As a consequence, the time-dependent isomerisation event would be enhanced at lower monomer concentrations where the time between each new docking event would be longer, thereby increasing the maturation time. However, our results showed that the impaired ability of $A\beta^{40WT}$ to bind to the fibrillar form of $A\beta^{40Arc}$ was not compensated for by lowering the monomer concentration. This suggests that the affinity between $A\beta^{40WT}$ monomers and the fibrillar end of $A\beta^{40Arc}$ is impaired. A direct measurement of the association between free $A\beta^{40WT}$ monomers and the fibrillar ends of $A\beta^{40Arc}$ was not possible due to a poor signal to noise ratio. The significantly higher dissociation rate noted upon probing $A\beta^{40}$ on $A\beta^{40Arc}$ fibrils, however, suggests a competing back-reaction and also a lower binding strength affinity. Competition studies between monomeric $A\beta^{40WT}$ and $A\beta^{40Arc}$ were performed as an alternative approach to evaluate the ability of $A\beta^{40WT}$ to bind to the fibrillar form of $A\beta^{40Arc}$. The results showed that $A\beta^{40WT}$ monomers are essentially unable to interfere with binding of $A\beta^{40Arc}$ to $A\beta^{40Arc}$ fibrils. However, $A\beta^{40WT}$ monomers affected the dissociation rate. This could possibly be the consequence of a small fraction of incorporated $A\beta^{40WT}$ monomers introducing weak links in the $A\beta^{40Arc}$ fibrils. This is consistent with a previous report where mixtures of $A\beta40^{Arc}$ and $A\beta^{40WT}$ stabilised the oligomeric state of $A\beta^{40Arc}$ and thereby prolonged its maturation into amyloid fibrils [30].

From our results, we can conclude that incorporation of $A\beta^{40WT}$ monomers into the fibrillar form of $A\beta^{40Arc}$ is significantly impaired as result of a reduced ability to dock and isomerise relative to $A\beta^{40Arc}$ monomers. Upon docking, the fibril structure is determined by a balance between intra-peptide and peptide-fibril interactions. At this point, it is not possible to determine if the impaired incorporation of $A\beta^{40WT}$ to adopt into $A\beta^{40Arc}$ fibrils is due to structural limitations of monomeric $A\beta^{40WT}$ in solution, interactions of the monomer with the fibril end or a combination of the two effects. Nonetheless, $A\beta^{40WT}$ monomer binding to $A\beta^{40Arc}$ is of low affinity and cannot compete efficiently with the $A\beta^{40Arc}$ monomer binding. Therefore, the properties of Aβ fibrils are controlled to a great extent by the properties and constraints of the precursor molecules.

From a general point of view, the initial formation of a nucleus and the architecture of the resulting amyloid fibrils are controlled by both thermodynamic and kinetic factors. As the aggregates increase in size, the energetic barriers between different states increases and kinetic barriers essentially block interconversion between different fibrillar forms. On this basis we hypothesise that the predominant fibrillar structure would be the structure with the fastest kinetics of formation even though more thermodynamically stable states might exist. Interestingly, this hypothesis is supported by the results shown here as the measurements of affinity between the monomers and the fibrillar ends are directly related to the thermodynamic stability of the fibril [27,28]. Our results show that

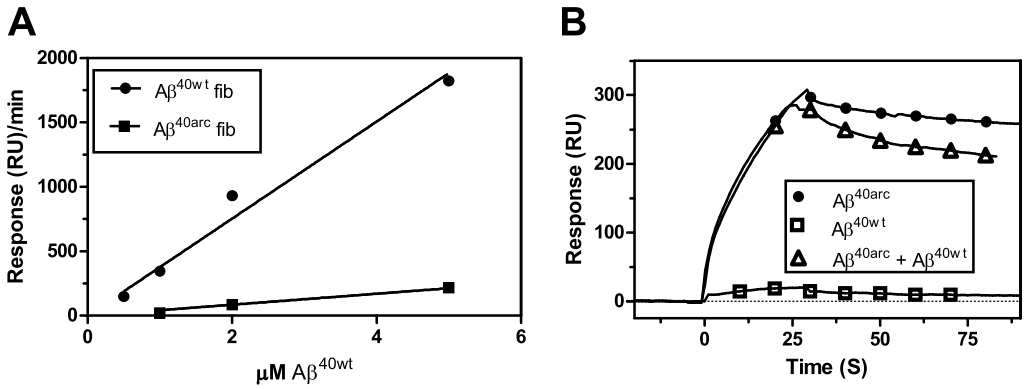

Figure 5. Competition between $A\beta^{40WT}$ and $A\beta^{40Arc}$ for polymerisation with $A\beta^{40Arc}$ or $A\beta^{40WT}$ fibrils. (A) Dose response for $A\beta^{40WT}$ binding to $A\beta^{40Arc}$ fibrils (filled squares) or $A\beta^{40WT}$ fibrils (filled circles). A range of concentrations of $A\beta^{40WT}$ were injected over $A\beta^{40Arc}$ or $A\beta^{40WT}$ fibrils in PBS at 25°C. The maximum response at the end of each injection was plotted against the concentration of $A\beta^{40WT}$. (B) Competition between $A\beta^{40WT}$ and $A\beta^{40Arc}$ for polymerisation to $A\beta^{40Arc}$ fibrils. $A\beta^{40WT}$ was injected for 30 s at a flow rate of 20 μl/min in PBS at 25°C. 5 μM $A\beta^{40Arc}$ (filled circles), 5 μM $A\beta^{40Arc}$+10 μM $A\beta^{40WT}$ (open triangles), 10 μM $A\beta^{40WT}$ (open squares).
doi:10.1371/journal.pone.0025157.g005

$A\beta^{40Arc}$ monomers have a significantly stronger affinity for $A\beta^{40WT}$ fibrils than $A\beta^{40Arc}$ fibrils. Since $A\beta^{40Arc}$ monomers can adopt the conformation of both $A\beta^{40WT}$ and $A\beta^{40Arc}$ fibrils, it is not thermodynamic stability that determines fibrillar architecture but rather the rate of formation. Due to the high kinetic barriers, a subsequent re-arrangement of the fibril into a thermodynamic more stable form is prevented.

Development of AD is the consequence of an imbalance between aggregate formation and degradation. The rate of peptide assembly as well as the stability of the formed aggregates is consequently of high importance. We can within this work show that the solvent protection patterns of the fibrillar forms of $A\beta^{40WT}$ and $A\beta^{40Arc}$ are similar and suggest a similar structure overall. However, through cross-seeding experiments, striking differences regarding aggregation rates was seen, indicating structural differences. Our results suggest that $A\beta^{40WT}$ docking and subsequent isomerisation into $A\beta^{40Arc}$ fibrils is restricted. This finding highlights the importance of structural constraints at an early point in the process of incorporating free monomers into Aβ fibrils. As a consequence, structural constraints of the monomer, possibly already in solution, determine the rate of fibril assembly. We further showed that formation of the predominant Aβ fibrillar architecture is controlled by kinetics rather than thermodynamics where the most thermodynamically stable form is not necessarily the predominant structure within a sample.

Acknowledgments

Alzheimerfonden, J.C. Kempe, the Swedish research council, O. E. och Edla Johanssons vetenskapliga stiftelse, FAMY Västerbotten, Stiftelsen AMYL and the Medical Faculty of Umeå University.

Author Contributions

Conceived and designed the experiments: AO AÖ KB. Performed the experiments: AO AÖ KB. Analyzed the data: AO AÖ KB. Contributed reagents/materials/analysis tools: AO AÖ KB. Wrote the paper: AO AÖ KB.

References

1. Ferri CP, Prince M, Brayne C, Brodaty H, Fratiglioni L, et al. (2005) Global prevalence of dementia: a Delphi consensus study. Lancet 366: 2112–2117.
2. Mercy L, Hodges JR, Dawson K, Barker RA, Brayne C (2008) Incidence of early-onset dementias in Cambridgeshire, United Kingdom. Neurology 71: 1496–1499.
3. Selkoe DJ (2001) Alzheimer's disease: genes, proteins, and therapy. Physiol Rev 81: 741–766.
4. Nilsberth C, Westlind-Danielsson A, Eckman CB, Condron MM, Axelman K, et al. (2001) The 'Arctic' APP mutation (E693G) causes Alzheimer's disease by enhanced Abeta protofibril formation. Nat Neurosci 4: 887–893.
5. Lord A, Englund H, Soderberg L, Tucker S, Clausen F, et al. (2009) Amyloid-beta protofibril levels correlate with spatial learning in Arctic Alzheimer's disease transgenic mice. FEBS J 276: 995–1006.
6. Johansson AS, Berglind-Dehlin F, Karlsson G, Edwards K, Gellerfors P, et al. (2006) Physiochemical characterization of the Alzheimer's disease-related peptides A beta 1–42Arctic and A beta 1–42wt. FEBS J 273: 2618–2630.
7. Whalen BM, Selkoe DJ, Hartley DM (2005) Small non-fibrillar assemblies of amyloid beta-protein bearing the Arctic mutation induce rapid neuritic degeneration. Neurobiol Dis 20: 254–266.
8. Sahlin C, Lord A, Magnusson K, Englund H, Almeida CG, et al. (2007) The Arctic Alzheimer mutation favors intracellular amyloid-beta production by making amyloid precursor protein less available to alpha-secretase. J Neurochem 101: 854–862.
9. Philipson O, Hammarstrom P, Nilsson KP, Portelius E, Olofsson T, et al. (2009) A highly insoluble state of Abeta similar to that of Alzheimer's disease brain is found in Arctic APP transgenic mice. Neurobiol Aging 30: 1393–1405.
10. Peralvarez-Marin A, Mateos L, Zhang C, Singh S, Cedazo-Minguez A, et al. (2009) Influence of residue 22 on the folding, aggregation profile, and toxicity of the Alzheimer's amyloid beta peptide. Biophys J 97: 277–285.
11. Knobloch M, Konietzko U, Krebs DC, Nitsch RM (2007) Intracellular Abeta and cognitive deficits precede beta-amyloid deposition in transgenic arcAbeta mice. Neurobiol Aging 28: 1297–1306.
12. Wirths O, Bethge T, Marcello A, Harmeier A, Jawhar S, et al. (2009) Pyroglutamate Abeta pathology in APP/PS1KI mice, sporadic and familial Alzheimer's disease cases. J Neural Transm 117: 85–96.
13. Codita A, Gumucio A, Lannfelt L, Gellerfors P, Winblad B, et al. (2010) Impaired behavior of female tg-ArcSwe APP mice in the IntelliCage: A longitudinal study. Behav Brain Res 215: 83–94.
14. Esler WP, Stimson ER, Jennings JM, Vinters HV, Ghilardi JR, et al. (2000) Alzheimer's disease amyloid propagation by a template-dependent dock- lock mechanism. Biochemistry 39: 6288–6295.
15. Cannon MJ, Williams AD, Wetzel R, Myszka DG (2004) Kinetic analysis of beta-amyloid fibril elongation. Anal Biochem 328: 67–75.
16. Aguilar MI, Small DH (2005) Surface plasmon resonance for the analysis of beta-amyloid interactions and fibril formation in Alzheimer's disease research. Neurotox Res 7: 17–27.
17. Hu WP, Chang GL, Chen SJ, Kuo YM (2006) Kinetic analysis of beta-amyloid peptide aggregation induced by metal ions based on surface plasmon resonance biosensing. J Neurosci Methods 154: 190–197.
18. Ryu J, Joung HA, Kim MG, Park CB (2008) Surface plasmon resonance analysis of Alzheimer's beta-amyloid aggregation on a solid surface: from monomers to fully-grown fibrils. Anal Chem 80: 2400–2407.

19. Olofsson A, Sauer-Eriksson AE, Ohman A (2006) The solvent protection of alzheimer amyloid-beta-(1–42) fibrils as determined by solution NMR spectroscopy. J Biol Chem 281: 477–483.
20. Olofsson A, Lindhagen-Persson M, Sauer-Eriksson AE, Ohman A (2007) Amide solvent protection analysis demonstrate that Amyloid-beta(1–40) and Amyloid-beta(1–42) form different fibrillar structures under identical conditions. Biochem J.
21. Ippel JH, Olofsson A, Schleucher J, Lundgren E, Wijmenga SS (2002) Probing solvent accessibility of amyloid fibrils by solution NMR spectroscopy. Proc Natl Acad Sci U S A 99: 8648–8653.
22. Olofsson A, Lindhagen-Persson M, Vestling M, Sauer-Eriksson AE, Ohman A (2009) Quenched hydrogen/deuterium exchange NMR characterization of amyloid-beta peptide aggregates formed in the presence of Cu2+ or Zn2+. FEBS J 276: 4051–4060.
23. Olofsson A, Sauer-Eriksson AE, Ohman A (2009) Amyloid fibril dynamics revealed by combined hydrogen/deuterium exchange and nuclear magnetic resonance. Anal Biochem 385: 374–376.
24. Lindhagen-Persson M, Brannstrom K, Vestling M, Steinitz M, Olofsson A (2010) Amyloid-beta oligomer specificity mediated by the IgM isotype–implications for a specific protective mechanism exerted by endogenous auto-antibodies. PLoS One 5: e13928.
25. Olofsson A, Lindhagen-Persson M, Sauer-Eriksson AE, Ohman A (2007) Amide solvent protection analysis demonstrates that amyloid-beta(1–40) and amyloid-beta(1–42) form different fibrillar structures under identical conditions. Biochem J 404: 63–70.
26. Myszka DG (1999) Improving biosensor analysis. J Mol Recognit 12: 279–284.
27. Williams AD, Shivaprasad S, Wetzel R (2006) Alanine scanning mutagenesis of Abeta(1–40) amyloid fibril stability. J Mol Biol 357: 1283–1294.
28. Williams AD, Portelius E, Kheterpal I, Guo JT, Cook KD, et al. (2004) Mapping abeta amyloid fibril secondary structure using scanning proline mutagenesis. J Mol Biol 335: 833–842.
29. Hasegawa K, Ono K, Yamada M, Naiki H (2002) Kinetic modeling and determination of reaction constants of Alzheimer's beta-amyloid fibril extension and dissociation using surface plasmon resonance. Biochemistry 41: 13489–13498.
30. Lashuel HA, Hartley DM, Petre BM, Wall JS, Simon MN, et al. (2003) Mixtures of wild-type and a pathogenic (E22G) form of Abeta40 in vitro accumulate protofibrils, including amyloid pores. J Mol Biol 332: 795–808.